JACS
JOURNAL OF THE AMERICAN CHEMICAL SOCIETY
Article
pubs.acs.org/JACS

Gd(III)-PyMTA Label Is Suitable for In-Cell EPR

Mian Qi,[||,†] Andreas Groß,[||,‡] Gunnar Jeschke,[§] Adelheid Godt,*[,†] and Malte Drescher*[,‡]

[†]Faculty of Chemistry and Center for Molecular Materials, Bielefeld University, Universitätsstraße 25, 33615 Bielefeld, Germany

[‡]Department of Chemistry, Zukunftskolleg, and Konstanz Research School Chemical Biology, University of Konstanz, Universitätsstraße 10, 78457 Konstanz, Germany

[§]Laboratory of Physical Chemistry, Department of Chemistry and Applied Biosciences, ETH Zurich, Vladimir-Prelog-Weg 2, 8093 Zurich, Switzerland

Supporting Information

ABSTRACT: Distance measurement in the nanometer range by electron paramagnetic resonance spectroscopy (EPR) in combination with site-directed spin labeling is a very powerful tool to monitor the structure and dynamics of biomacromolecules in their natural environment. However, in-cell application is hampered by the short lifetime of the commonly used nitroxide spin labels in the reducing milieu inside a cell. Here, we demonstrate that the Gd(III) based spin label Gd-PyMTA is suitable for in-cell EPR. Gd-PyMTA turned out to be cell compatible and was proven to be inert in in-cell extracts of *Xenopus laevis* oocytes at 18 °C for more than 24 h. The proline rich peptide H-AP$_{10}$CP$_{10}$CP$_{10}$-NH$_2$ was site-directedly spin labeled with Gd-PyMTA at both cysteine moieties. The resulting peptide, H-AP$_{10}$C(Gd-PyMTA)P$_{10}$C(Gd-PyMTA)P$_{10}$-NH$_2$, as well as the model compound Gd-spacer-Gd, which consists of a spacer of well-known stiffness, were microinjected into *Xenopus laevis* oocytes, and the Gd(III)−Gd(III) distances were determined by double electron−electron resonance (DEER) spectroscopy. To analyze the intracellular peptide conformation, a rotamer library was set up to take the conformational flexibility of the tether between the Gd(III) ion and the C_α of the cysteine moiety into account. The results suggest that the spin labeled peptide H-AP$_{10}$C(Gd-PyMTA)P$_{10}$C(Gd-PyMTA)P$_{10}$-NH$_2$ is inserted into cell membranes, coinciding with a conformational change of the oligoproline from a PPII into a PPI helix.

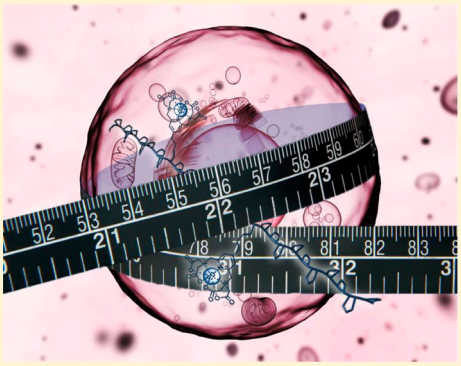

INTRODUCTION

The determination of structure and dynamics of biomacromolecules such as proteins in their natural environment by intracellular spectroscopy is crucial for understanding their function.[1−11] A very powerful tool to gain information on structure and dynamics of biomolecules *in vitro*[12−14] is a particular technique in electron paramagnetic resonance (EPR) spectroscopy: the four-pulse DEER (double-electron−electron-resonance) measurement, which yields precise distances and distance distributions in the nanometer range.[15−20] To apply this technique, two paramagnetic labels, so-called spin labels, are attached at selected sites of the biomolecule (site-directed spin labeling, SDSL) and the dipolar coupling between the two paramagnetic centers is measured.[13,16,21−32] The dipolar coupling is inversely proportional to the cube of the distance and thus contains structural information.[33,34] Unfortunately, in-cell application[35−39] is so far very limited because the nitroxides, the commonly used spin labels, are converted rather rapidly into diamagnetic, and therefore EPR silent, hydroxylamines when exposed to the reductive environment inside a cell.[37,40] Shock-freezing of the sample, as usually applied for the DEER measurement, inhibits spin label reduction. Nevertheless, the spin labels are exposed to the reductive conditions at physiological temperature during the time span (incubation time) that is needed by the biomacromolecule to attain its native shape, which may take hours.[41,42]

A recent addition to the set of spin labels are complexes of gadolinium in the oxidation state +3. Gd(III) complexes are also used as contrast agents for magnetic resonance imaging (MRI),[43] and a multitude of bioconjugated Gd(III) complexes are known to choose from.[43−46] They offer several advantages in comparison to nitroxides, e.g. the absence of orientation selection, enabling accurate DEER distance measurements at high fields/frequencies, higher transition moments owing to the high spin system of $S = 7/2$, fast shot repetition rates at lower temperatures due to the short longitudinal relaxation time (T_1), and, additionally, broadening of the type of EPR techniques.[47,48] Goldfarb and Raitsimring et al. demonstrated their usability for DEER on several model systems, proteins, peptides, and DNA in *in vitro* experiments; albeit, the details of how to extract the distance distribution from the experimentally determined dipolar coupling still awaits an in-depth understanding.[48−53] During the review process for this article, an article appeared by Martorana et al. on in-cell DEER studies of Gd(III) labeled ubiquitin.[54]

Received: August 17, 2014
Published: October 7, 2014

   dx.doi.org/10.1021/ja508274d | J. Am. Chem. Soc. 2014, 136, 15366−15378

Gd(III) complexes also caught our interest because we expected the Gd(III) ion to withstand the reducing conditions inside a cell. Although Gd(III) is highly toxic, its toxicity is significantly reduced upon complexation.[43,55−57] Indeed, as shown below, experiments proved the complex Gd-PyMTA[58] to be inert in the cell extract of *Xenopus laevis* oocytes for at least 24 h at 18 °C and the morphology of *Xenopus laevis* oocytes that had been loaded with Gd-PyMTA labeled molecules to stay unchanged for at least 3 h at 18 °C. To further explore the applicability of Gd(III) complexes for in-cell DEER measurements, the proline rich peptide H-$AP_{10}CP_{10}CP_{10}$-NH_2 (peptide **7**) was labeled with the Gd(III) complex Gd-PyMTA, using the two thiol groups of the peptide as covalent anchors and the decaproline segment as a spacer. Due to its stiffness, polyproline is a commonly used peptide for the test of distance determination methods.[59,60] The spin labeled peptide H-AP_{10}C(Gd-PyMTA)P_{10}C(Gd-PyMTA)P_{10}-NH_2 (peptide **9**) was microinjected into *Xenopus laevis* oocytes. Subsequent DEER experiments demonstrated that Gd-PyMTA is well suited for in-cell application. Corresponding experiments with Gd-spacer-Gd (**10**), a model compound featuring two Gd-PyMTA moieties separated by a rodlike spacer, showed that accurate in-cell EPR distance measurements are possible in the presence of endogenous paramagnetic centers in the cell, in particular Mn(II) species.

The tether between the Gd(III) ion and the C_α of the cysteine moiety in peptide **9** was kept as short as possible—approximately 12 Å—to facilitate the interpretation of distance measurements. Nevertheless, its conformational flexibility affects the experimentally determined distance distribution. To account for this influence, a rotamer library[61] for the PyMTA-label was generated.

We applied the Gd(III)-label based in-cell EPR approach to study the conformation of a proline rich peptide *in cellula*. Our data suggest that this peptide is partially localized in membranes and undergoes a conformational transition from a polyproline helix type II (PPII) into a type I helix (PPI) inside the oocyte. This process occurs on a time scale between minutes and hours, making the long time stability of the spin labels as offered by Gd-PyMTA inevitable for monitoring the conformational change by in-cell EPR. The fact that this PPII to PPI transition is found only under *in vivo* conditions but not in cell extract offers explicit motivation for *in vivo* studies.

The paper presents our exploration of Gd-PyMTA as a spin label for in-cell EPR. It is organized as follows. In the first part, the synthesis of the ligand 4-vinyl-PyMTA and of its Gd(III) complex, studies on the selectivity of 4-vinyl-PyMTA for cysteine, the resistance of the Gd-PyMTA complex against reduction in cell extract, and the spin labeling of peptide H-$AP_{10}CP_{10}CP_{10}$-NH_2 (peptide **7**) to obtain H-AP_{10}C(Gd-PyMTA)P_{10}C(Gd-PyMTA)P_{10}-NH_2 (peptide **9**) are presented. In the second part, the results of Q-band DEER measurements of Gd-spacer-Gd (**10**) and of peptide **9** in deuterated aqueous solution as well as inside *Xenopus laevis* oocytes are presented together with rotamer library based simulations of the distance distributions indicating a cell membrane induced PPII to PPI transition.

RESULTS AND DISCUSSION

Synthesis. The most common spin-labeling strategy for proteins uses cysteine substitution mutagenesis in combination with a spin label that selectively forms a covalent bond with the thiol group of the cysteine moiety.[13,62,63]. To make the application of Gd(III) complexes fitting to this standard and widely used site-directed labeling protocol, we selected the 4-vinyl-PyMTA (**3**)[64] for attaching the Gd(III) to the peptide. 4-Vinyl-PyMTA (**3**) was recently introduced by Yang et al. as a tag in site-specific labeling of proteins with lanthanides for structure analysis with NMR-spectroscopic experiments.[64] PyMTA forms highly stable complexes with Gd(III) (log K ∼ 19).[58,65] The Michael addition of the thiol group of the cysteine residue to the vinyl group of the 4-vinyl-PyMTA (**3**) results in a thioether linkage that we expected to be stable in the cellular environment.

Synthesis of 4-vinyl-PyMTA (3) and Gd-4-vinyl-PyMTA (4). Yang et al. obtained 4-vinyl-PyMTA (**3**) through a Hiyama coupling between 4-bromo-PyMTA tetraethyl ester and triethoxyvinylsilane, subsequent ester hydrolysis, and finally protonation using a proton-exchange resin.[64] We have prepared 4-vinyl-PyMTA (**3**) starting from 4-iodo-PyMTA tetraethyl ester (**1**) and using a Molander type Suzuki coupling with potassium vinyltrifluoroborate[66] (Scheme 1), giving 4-vinyl-PyMTA tetraethyl ester (**2**). Compared to the Hiyama coupling, the Molander type Suzuki coupling gave a significantly higher yield (82% vs 52%). Ester hydrolysis following the protocol of Yang et al.[64] provided us with 4-vinyl-PyMTA (**3**).

The 4-vinyl-PyMTA (**3**) made on this route contains about 2 mol % of an unidentified organic compound (Figure S10,b) and, as indicated by the elemental analysis, about 10 wt % of inorganic matter. The latter suggests that ion exchange was incomplete (for details see Supporting Information). The organic bycomponent was contained in the material made by Yang et al. as well (see Figures 2 and S1 in ref 64). Neither the organic bycomponent nor the inorganic matter interfere with the labeling reaction, as shown below. Notably, our ^{1}H NMR spectroscopic data of 4-vinyl-PyMTA ester **2** and 4-vinyl-PyMTA (**3**) deviate substantially from the data reported by Yang.[64] No further NMR data have been published. All our NMR data (^{13}C NMR data and 2D NMR data) as well as mass spectrometric data and the elemental analysis of 4-vinyl-PyMTA ester **2** are in agreement with the structural formulas shown in Scheme 1.

Addition of $GdCl_3$ to 4-vinyl-PyMTA (**3**) in water and subsequently raising the pH to 7.2 through the addition of aqueous NaOH gave the complex Gd-4-vinyl-PyMTA (**4**). This complex was used to test the stability of Gd-PyMTA toward the reducing conditions of the cell environment. Please note that it is of importance to first mix $GdCl_3$ and 4-vinyl-PyMTA (**3**) in water before adding the aqueous NaOH. Otherwise, the Gd(III) precipitates as $Gd(OH)_3$.

Selectivity of 4-vinyl-PyMTA toward amino acids. For the use of 4-vinyl-PyMTA (**3**) as a spin label for proteins, the selectivity for cysteine is of utmost importance. Yang et al. reported tests on the reactivity of cysteine, methionine, and lysine in a phosphate buffer at pH 7.5 and at room temperature using an excess (3−10 equiv) of the amino acids.[64] The reaction with cysteine was complete within 6 h, and no reaction was detected with lysine and methionine within 24 h. We studied the reaction rate of 4-vinyl-PyMTA (**3**) with cysteine, alanine, lysine, histidine, arginine, and proline in Tris-HCl buffer [$H_2NC(CH_2OH)_3$-HCl buffer] at pH 7.8 (Table 1, Figure S2−S7) at 25 °C and at 40 °C. 4-Vinyl-PyMTA (**3**) is stable under these conditions for at least 144 h (Table 1, entries 1 and 11). The molar ratios of the amino acid and 4-vinyl-PyMTA (**3**) were 1:1. Cysteine reacted quickly at room

dx.doi.org/10.1021/ja508274d | J. Am. Chem. Soc. 2014, 136, 15366−15378

Scheme 1. Synthesis of 4-Vinyl-PyMTA (3) through a Molander Type Suzuki Coupling and the Formation of Gd-4-vinyl-PyMTA (4)

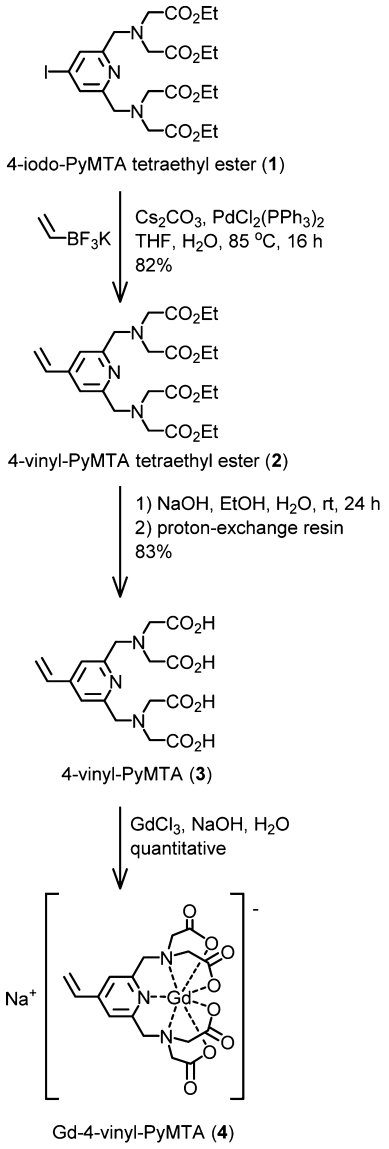

temperature (Table 1, entries 2–5). The conversion came close to 90% within 6 h and was found to be quantitative after 24 h. We have no data between 6 and 24 h. At 40 °C, 6 h was sufficient to achieve nearly complete labeling (96%) of cysteine (Table 1, entries 12–15). Alanine did not react with 4-vinyl-PyMTA (3) at room temperature and only extremely slowly at 40 °C (Table 1, entries 6 and 16), indicating that the NH_2-group at the end of a protein is almost inert. The amino acids lysine, histidine, arginine, and proline reacted with an increasing rate in this order, but only very slowly at 25 °C (Table 1, entries 7–10). The conversions were around 1–2% after 144 h. At 40 °C the conversion ranged from 3 to 6% for a reaction time of 144 h (Table 1, entries 17–20). The experiments prove the high selectivity of 4-vinyl-PyMTA (3) for cysteine. However, other amino acids are not completely inert toward 4-vinyl-PyMTA (3), a finding that needs to be kept in mind if the cysteine residues of a protein are not easily accessible and therefore a long reaction time or a temperature above room temperature is needed. Another important result of these

Table 1. Reaction of 4-Vinyl-PyMTA (3) with Amino Acids[a]

entry	4-vinyl-PyMTA (3) [μmol]	amino acid	[μmol]	T [°C]	t [h]	conversion of 4-vinyl-PyMTA (3)
1	28.0			25	144	0%
2	27.8	L-cysteine	28.1	25	2	69%
3	27.8	L-cysteine	28.1	25	4	81%
4	27.8	L-cysteine	28.1	25	6	87%
5	27.8	L-cysteine	28.1	25	24	100%
6	28.4	L-alanine	31.4	25	240	0%
7	27.5	L-lysine	27.4	25	144	1.1%
8	27.4	L-histidine	27.1	25	144	1.3%
9	28.0	L-arginine	28.0	25	144	1.6%
10	28.0	L-proline	27.8	25	144	1.9%
11	28.0			40	144	0%
12	28.0	L-cysteine	28.0	40	2	84%
13	28.0	L-cysteine	28.0	40	4	94%
14	28.0	L-cysteine	28.0	40	6	96%
15	28.0	L-cysteine	28.0	40	24	100%
16	28.4	L-alanine	31.4	40	144	1.1%
17	27.2	L-lysine	27.1	40	144	3.2%
18	27.0	L-histidine	26.7	40	144	3.6%
19	27.6	L-arginine	27.6	40	144	3.9%
20	27.5	L-proline	27.3	40	144	5.3%

[a]In NMR tubes the amino acid and 4-vinyl-PyMTA (3) were dissolved in Tris-HCl buffer (pH 8.0, 0.05 M, 0.6 mL) and the pH of the solution was adjusted to 7.8 through the addition of Tris or HCl. The conversion of 4-vinyl-PyMTA (3) was followed by ^{1}H NMR spectroscopy using water-suppression by a presaturation technique.[67] The signal of Tris was used as an internal standard with δ = 3.52 ppm (For ^{1}H NMR spectra see Figures S2–S7).

studies is that the unidentified organic component accompanying 4-vinyl-PyMTA (3) did not react. This was deduced from the ^{1}H NMR spectra which show that the relative intensity of the signal of this bycomponent stayed constant (Figures S2–S7).

Stability of Gd-4-vinyl-PyMTA (4) in cell extract. The stability of Gd-4-vinyl-PyMTA (4) in cell extract (*Xenopus* cytostatic factor arrested, CSF) was tested through monitoring Gd-4-vinyl-PyMTA (4) with X-band cw-EPR spectroscopy at 18 °C (Figure 1). The shape and intensity of the EPR signal remained constant for more than 24 h, indicating that the complex is stable and no release of Gd out of the complex can be observed. In contrast, the signal intensity of 3-(carboxy)-

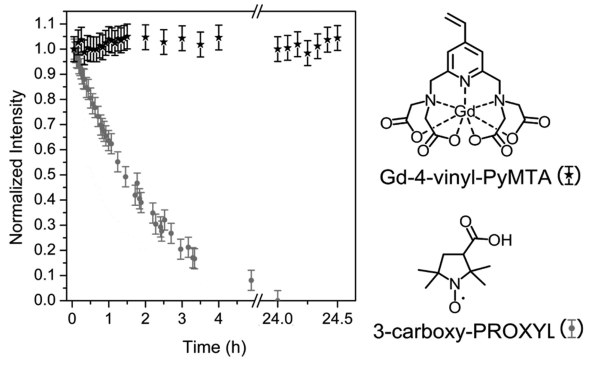

Figure 1. Time-dependent EPR signal intensity of Gd-4-vinyl-PyMTA (4) (black stars) and 3-carboxy-PROXYL (gray dots) in a cell extract of *Xenopus laevis* oocytes (1:3) at 18 °C (start: 500 μM concentration).

dx.doi.org/10.1021/ja508274d | J. Am. Chem. Soc. 2014, 136, 15366–15378

2,2,5,5-tetramethyl-1-pyrrolidinyloxy (3-carboxy-PROXYL), a model for the commonly used nitroxide labels, decayed with a half-life time of 85 min at 18 °C (Figure 1). Thereby, the spectral shape remained unchanged, indicating that the reduction of the nitroxide was effective under the applied conditions.

Labeling of the peptide H-AP$_{10}$CP$_{10}$CP$_{10}$-NH$_2$ (peptide 7). To test the applicability of Gd-PyMTA as a spin label for in-cell application, we spin labeled a peptide with the sequence H-AP$_{10}$CP$_{10}$CP$_{10}$-NH$_2$ (peptide **7**). As shown in Table 1, the amino group of proline reacts slowly with 4-vinyl-PyMTA (**3**) at 40 °C, whereas alanine is essentially inert under these conditions. Suitably, the N-terminal amino acid of peptide **7** is alanine.

In site-directed labeling, it is common to apply a reducing agent for disulfides, e.g. tris(2-carboxyethyl)phosphine (TCEP).[68,69] This agent has been applied by Yang et al. when labeling a protein with 4-vinyl-PyMTA (**3**).[64] We found that under the labeling conditions (pH 7.8, Tris-HCl buffer, room temperature) TCEP reacts fast and quantitatively with 4-vinyl-PyMTA (**3**), forming the TCEP adduct **5** (Figure S1,b). A competition reaction between equal molar amounts of TCEP and cysteine for 4-vinyl-PyMTA (**3**) at pH 7.8 and room temperature gave a 57:43 mixture of TCEP adduct **5** and cysteine adduct **6** (Scheme 2, Figure S1,c). Obviously, TCEP competes efficiently with cysteine for 4-vinyl-PyMTA (**3**). Therefore, when needing a reducing agent, the amount of TCEP should be kept to a minimum.

Scheme 2. Competition of TCEP and Cysteine (1:1 ratio) for 4-Vinyl-PyMTA (3) in an Aqueous Solution at pH 7.8 (Tris-HCl buffer) and Room Temperature, Revealing That TCEP Reacts with 4-Vinyl-PyMTA Even a Little Faster than Cysteine

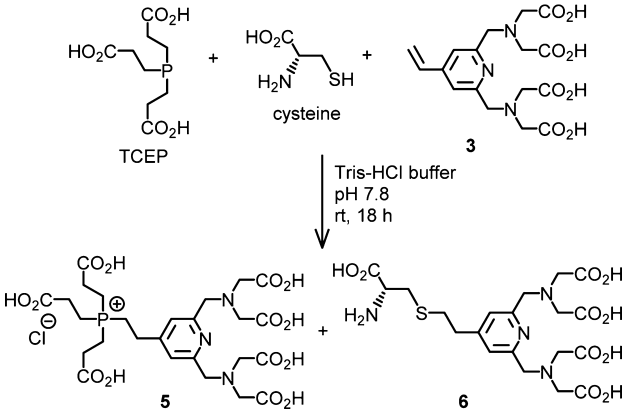

Peptide **7**, H-AP$_{10}$CP$_{10}$CP$_{10}$-NH$_2$, was labeled with Gd-PyMTA in two steps: (1) attachment of the ligand and (2) complexation of Gd(III) ions (Scheme 3). The ligand attachment was performed under argon to avoid the formation of disulfide and thus the need for TCEP or other reducing agents that compete with cysteine for the ligand. The progress of the ligand attachment was followed by HPLC-MS. It was surprisingly slow. Even at 40 °C, it took about 80 h to come to completion. That the reaction of a cysteine being part of a protein with 4-vinyl-PyMTA (**3**) is slower than that of cysteine was also found by Yang et al. However, the peptide **7** reacted even much more slowly than the protein used in the study of

Scheme 3. Site-Directed Spin Labeling of Peptide 7

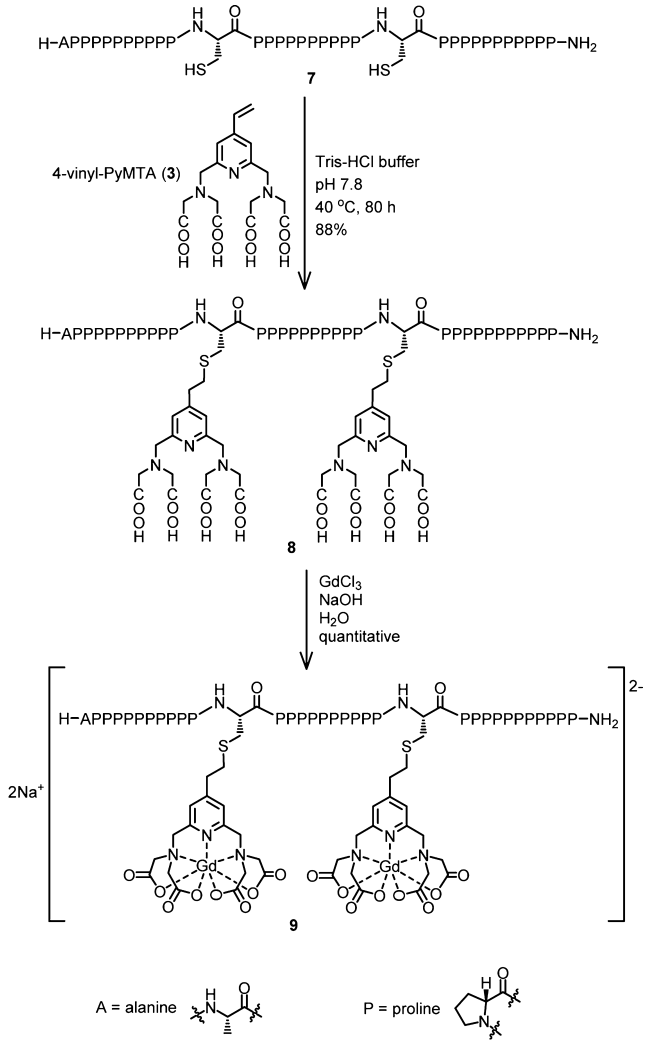

Yang et al., who report the reaction to be quantitative within 24 h at room temperature and pH 7.8.[64]

The ligand carrying peptide **8** was isolated by HPLC and loaded with two Gd(III) ions to obtain spin labeled peptide **9**, H-AP$_{10}$C(Gd-PyMTA)P$_{10}$C(Gd-PyMTA)P$_{10}$-NH$_2$.

Endogenous paramagnetic species in *Xenopus laevis* oocytes. Intracellular distance measurements of nitroxide labeled DNA and proteins have been performed by DEER after microinjection into *Xenopus laevis* oocytes.[35−39] Microinjection of *Xenopus laevis* has been established as a standard protocol for in-cell EPR, whereby the sample solution is injected into the relatively large oocytes (approximately 1 mm in diameter) followed by shock-freezing after the desired incubation time.[35,37,40,70] The EPR spectrum of untreated oocytes (Figure 2) consists of a characteristic signal of six lines of an endogenous Mn(II) species and of a signal featuring one EPR line of endogenous radicals at B = 12130 G.[71] Spectral simulations revealed an effective spin concentration of approximately 10 μM Mn(II) inside the cell (Figure S14). An Mn(II)-DEER experiment shows that the experimental data can be described by a homogeneous three-dimensional distribution of Mn(II) species inside the cell (Figure S15). Hence, the Mn(II) signal should not affect experimentally obtained distance distributions *in cellula*; however, the modulation depth and, as a result, signal-to-noise ratio (SNR)

dx.doi.org/10.1021/ja508274d | J. Am. Chem. Soc. 2014, 136, 15366−15378

of the dipolar evolution curves will be reduced as the Mn(II) contributes to the background of the DEER measurement.

Model system Gd-spacer-Gd (10). In order to prove that accurate distance measurements *in cellula* are possible in spite of the endogenous paramagnetic species, we employed a model containing two Gd(III)-PyMTA complexes held at a distance of about 3.1 nm (Gd−Gd distance) by a rodlike spacer. The stiffness of the spacer is limited but well-known,[20,33] and this type of spacer has been extensively used in methodological studies of EPR distance measurements.[20,33,50] For this study, branched oligo(ethylene glycol) substituents were attached to the spacer in order to obtain a water-soluble compound.

Figure 2 shows the echo-detected field sweep of Gd-spacer-Gd (**10**) in D_2O (30 vol % glycerin-d_8) at Q-band (34 GHz; T = 10 K). The broad spectrum originates from the entity of all spin transitions and contains the central transition ($S = -1/2 \rightarrow +1/2$).[50]

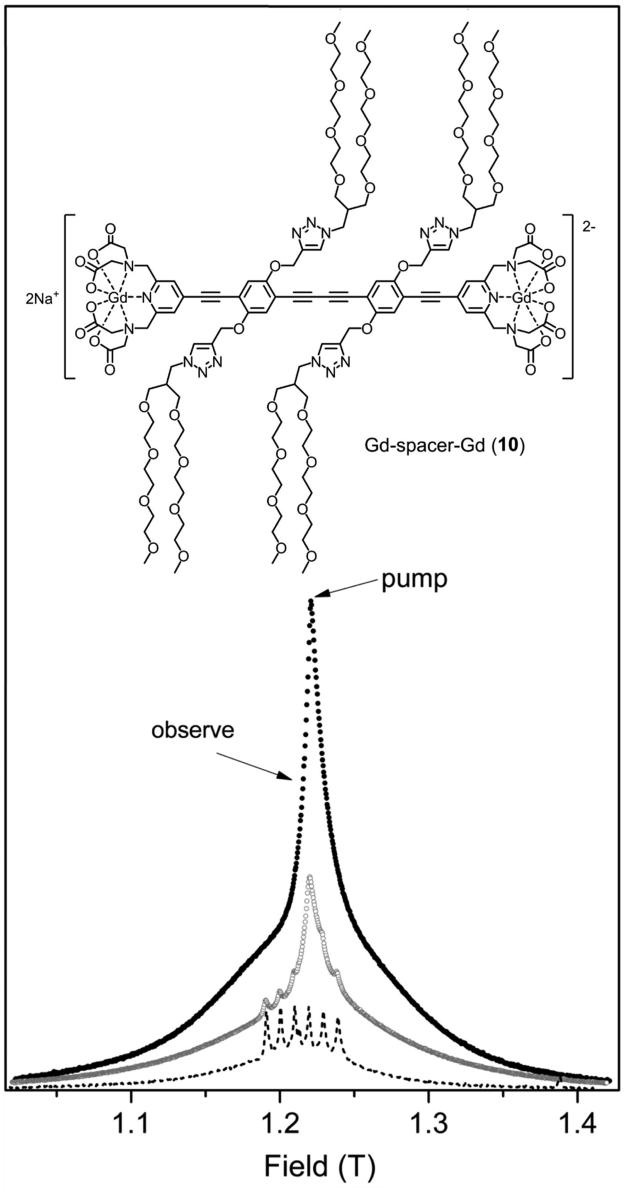

Figure 2. Q-band two-pulse echo-detected field sweeps of untreated, pulverized oocytes (dashed line) and of the water-soluble Gd-spacer-Gd (**10**) in D_2O (30 vol % glycerin-d_8) (black dots) and inside *Xenopus laevis* oocytes (circles) (τ = 400 ns, 10 K). Arrows indicate positions of pump and observer pulses of the corresponding DEER experiment ($\Delta\upsilon$ = 150 MHz).

Q-band (34 GHz) DEER measurements of Gd-spacer-Gd (**10**) in D_2O (30 vol % glycerin-d_8) were carried out at T = 10 K. The experimental data and background corrected time trace are shown in Figure 3. The modulation depth λ of 0.04 is, as expected, taking the spectral width of the central transition and the used pump pulse length of 16 ns into account.[50] The displayed fit originates from a model-free Tikhonov regularization (for the choice of the α-parameter, see Figure S16). The resulting distance distribution is shown in Figure 3. The mean distance of 3 nm is in accordance with the Gd−Gd distance of 3.1 nm, which was estimated based on the length of the individual bonds.[20,33,50] The half width at half-maximum of 6.5 Å is larger than expected. For a structurally very similar compound—the same spacer but with nitroxide instead of Gd-PyMTA as the spin label—a distribution for the electron-to-electron distance with a half width at half-maximum of only 1 Å was determined.[20,33] As pointed out by Goldfarb et al. for a shorter homologue of Gd-spacer-Gd (**10**),[50] the distance distribution in the case of Gd-spacer-Gd (**10**) may partly be due to a dislocation of the Gd(III) ion from the plane of the pyridine ring caused by solvation and counterion effects. As a result of this dislocation, the Gd−Gd connecting line no longer coincides with the long axis of the spacer. Therefore, the free rotation around the CC single bonds of the spacer backbone permits conical rotation of the Gd(III) ions around the spacer axis, thus giving rise to multiple distances despite the rather stiff[20,33] spacer backbone. Furthermore, due to a small D value of the zero field splitting (ZFS), the weak coupling approximation of the spin pair does not apply any longer.[48] Therefore, frequencies will occur in the dipolar evolution curve, which are not equal to the dipole−dipole interaction frequency (ω_{dd}) and lead to an artificial broadening of the extracted distance distributions.[48]

In-cell EPR distance measurements of Gd-spacer-Gd (10). Stage V/VI oocytes were visually checked and microinjected with 50 nL of 8 mM Gd-spacer-Gd (**10**) dissolved in H_2O. Carefully applied negative pressure was used to pull three oocytes into the EPR test tube without harming the vitelline membrane. The oocytes were kept for a specific time (incubation time) at 18 °C, then shock-frozen, and stored at −80 °C. During the incubation, the oocytes were visually inspected under a binocular microscope. Their morphological stability upon microinjection of the Gd-spacer-Gd (**10**) solution amounts to at least 3 h of incubation at 18 °C (Figure 4), whereas the microinjection of pure buffer (Tris-HCl in D_2O (pH 7.4)) results in an oocyte lifetime of 10−12 h. For incubation times exceeding the above-mentioned, we observed apoptotic cells, severe leakage, and complete disruption of the membrane (Figure 4). Although the lifetime of oocytes loaded with Gd-spacer-Gd (**10**) and the even longer lifetime of Gd(III)-PyMTA in the cellular milieu would have allowed for longer incubation times, we chose an incubation time of 1 h to ensure that all cells in the sample were still intact.

Figure 2 shows the corresponding field sweep of Gd-spacer-Gd (**10**) *in cellula* after 1 h of incubation at 18 °C. The received spectrum is a superposition of the signal of Gd-spacer-Gd (**10**) and the signal of untreated oocytes.

DEER measurements of Gd-spacer-Gd (**10**) inside *Xenopus laevis* oocytes were performed at Q-band at T = 10 K. The local Gd(III) concentration was determined by DEER to be 1250

dx.doi.org/10.1021/ja508274d | J. Am. Chem. Soc. 2014, 136, 15366−15378

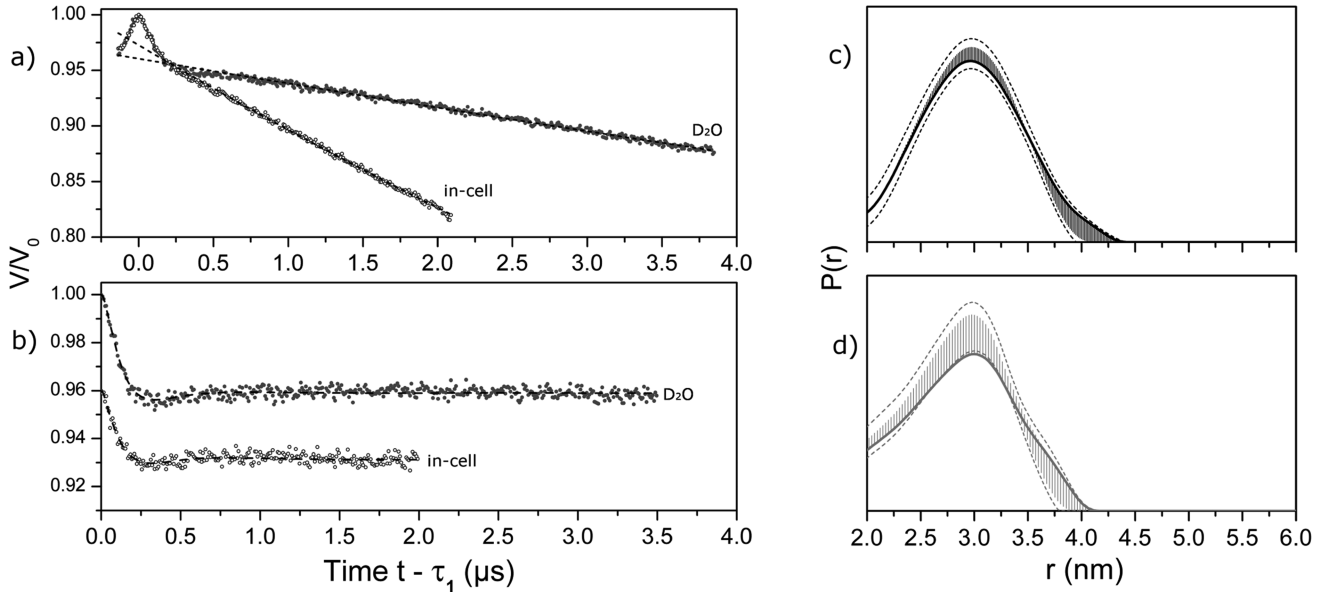

Figure 3. (a) Four-pulse DEER-traces of Gd-spacer-Gd (**10**) in D_2O (30 vol % glycerin-d_8) (black dots) and inside *Xenopus laevis* oocytes after 1 h of incubation time (circles) recorded at Q-band (T = 10 K) and corresponding background fits (dashed lines), assuming a homogeneous 3D distribution of molecules; (b) Background-corrected DEER curves of the corresponding experiments with Tikhonov regularization fit; observer pulses 16/16/32 ns, pump pulse 16 ns, $\Delta\upsilon$ = 150 MHz, accumulation time 2 h (black dots, D_2O) or 18 h (circles, in-cell); (c) Distance distributions obtained via Tikhonov regularization of the corresponding DEER-traces of Gd-spacer-Gd (**10**) in D_2O (30 vol % glycerin-d_8) and (d) inside *Xenopus laevis* oocytes (solid line). The error bars are the full variation of the probability of given distances obtained during the statistical analysis (see Experimental Methods), whereas the dotted lines are upper/lower error estimations corresponding to the mean value ± two times the standard deviation of the different Tikhonov fits.

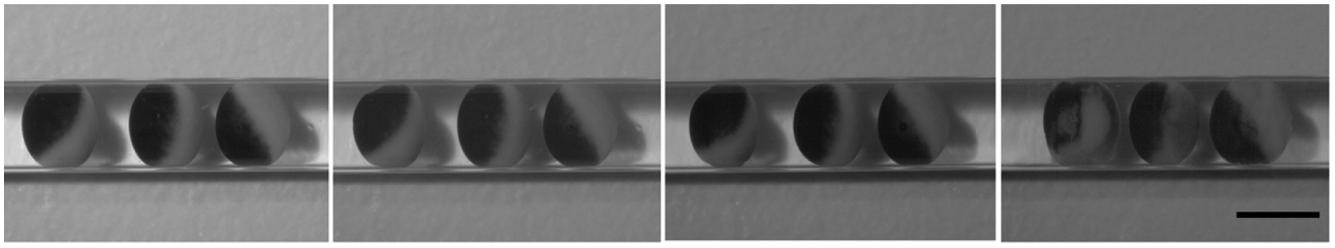

Figure 4. From left to right: Micrographs of *Xenopus laevis* oocytes after incubation at T = 18 °C for 5 min, 1 h, 3 h, and 4 h after microinjection of 50 nL of an 8 mM solution of Gd-spacer-Gd (**10**) in H_2O. Scale bar = 1 mm.

μM.[72] This concentration differs from the effective concentration of 210 μM, as was determined from the field sweeps. The difference cannot be explained by the partial filling of the sample tube, only. Therefore, an inhomogeneous distribution of the Gd-spacer-Gd (**10**) inside the cell is assumed (see Table S1). The endogenous cellular EPR signal at the observer frequency and the larger width of the Gd(III) spectrum *in cellula* than in D_2O leads to a lower modulation depth λ of 0.03 in the background corrected dipolar evolution curve in comparison to the corresponding measurement in D_2O (Figure 3). Taking these factors into account, a corrected modulation depth λ_{corr} of 3.7% was calculated, which is in good accordance with the measured λ = 4% of Gd-spacer-Gd (**10**) in D_2O (Table S1), indicating that no significant fraction of Gd is released from the complex. Furthermore, the transverse relaxation time (T_2) of the Gd(III) complex is reduced 3.4 times to 1.4 μs compared to T_2 in D_2O. Both effects—reduced modulation depth as well as reduced transverse relaxation time—result in a worse signal-to-noise ratio of the dipolar evolution curve and forced an overall shorter DEER evolution time compared to the measurement in D_2O. This 1.6 times worse SNR compared to the DEER trace of Gd-spacer-Gd in D_2O is also reflected by the accuracy of the obtained distance distribution shown in Figure 3. Although the estimated error of the distance distribution is more distinct, the comparison with the distance distribution received for Gd-spacer-Gd (**10**) in D_2O reveals strong similarity of the distance distributions in D_2O and *in cellula*, proving that accurate intracellular EPR distance measurements using Gd-PyMTA are feasible.

EPR distance measurements on peptide 9. The high content of proline in peptide **9** suggests that a polyproline helix II (PPII) will be formed in aqueous solution, which is a left-handed helix with an axial translation of 0.31 nm per residue. The high conformational stability and rigidity of the PPII helix *in vitro* has led to its repeated use as a molecular ruler in several applications.[59,60]

The data obtained for peptide **9** in deuterated Tris-HCl buffer (30 vol % glycerin-d_8) fit well to this expectation. The background corrected DEER curve of peptide is shown in Figure 5 (raw data and field sweep, see Figures S17−S19), featuring a modulation depth of λ = 0.024, which is lower than expected from spectral shape and pulse lengths. Reduced modulation depths for Gd(III) distance measurements have already been observed.[50]

dx.doi.org/10.1021/ja508274d | J. Am. Chem. Soc. 2014, 136, 15366−15378

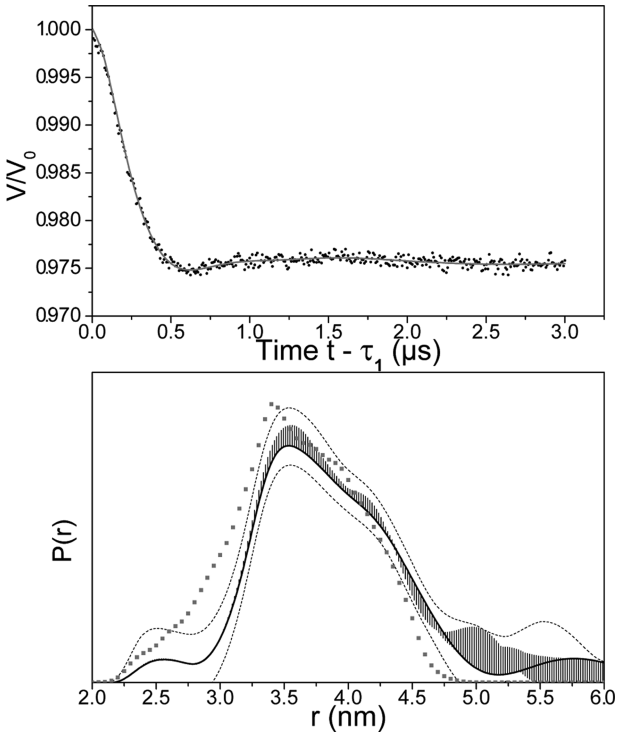

Figure 5. Top: Background corrected four-pulse DEER trace of peptide **9** in deuterated buffer (30 vol % glycerin-d_8) (black dots) and Tikhonov regularization fit (gray dotted line) recorded at Q-band, 10 K; observer-pulses 16/16/32 ns, pump-pulse 16 ns, $\Delta\upsilon$ = 120 MHz, accumulation time 12 h. Bottom: Mean distance distributions obtained via Tikhonov regularization of the DEER trace (solid line) together with the distance distribution calculated for a corresponding model of a PPII helix (squares) with MMM (see Figure 6). The error bars are the full variation of the probability of given distances obtained during the statistical analysis (see Experimental Methods), whereas the dotted lines are upper/lower error estimations corresponding to the mean value ± two times the standard deviation of the different Tikhonov fits.

Figure 5 shows the resulting distance distribution. Contributions to this distance distribution below approximately 3 nm are nonsignificant, as indicated by the lower error estimation placed at zero probability. The simulated distance distribution (squares) has been obtained on the basis of a PPII helical conformation (Figure 6) with the dihedral angles of ϕ = −75°, ψ = 160°, and ω = 0° for all residues. The flexibility of the tether between Gd(III) and the C_α of the cysteine moiety was taken into account by a rotamer library approach, which has been implemented in MMM2013.2.[61] Briefly, the complex geometry was optimized by density functional theory and the conformational distribution of the label linker was determined by Monte Carlo sampling with fixed bond lengths and angles, considering only the torsion and nonbonding interaction potentials of the universal force field (UFF).[73] An ensemble of 20,000 low-energy conformations was reduced by hierarchical clustering to the 324 rotamers expected from multiplicity of the torsion potentials. In computing of the conformational distribution of the label attached to the PPII helix, UFF nonbonding energy between label and peptide atoms is considered. Even if it is possible and maybe even likely that the cysteine residues will not adopt the same dihedral angles as the proline residues, leading to kinks in the helical structure at these specific residues, the model is featuring a good approximation in the homogeneous proline region between the two cysteine residues.[74] Conformational uncertainty at the cysteine residues is expected to have only a weak influence on the distance of the two labels attached to the cysteines; the additional proline residues before and after the measured area are of use to design the molecular weight, lipophilicity, and water solubility of such a 33-residues-long, proline rich peptide. The simulation suggests that the width of the distance distribution originates rather from the flexibility of the spin label tether than from the (conformational) flexibility of the peptide itself occurring in a single conformation.

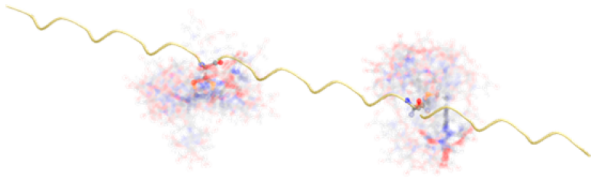

Figure 6. Model of H-$AP_{10}C$(Gd-PyMTA)$P_{10}C$(Gd-PyMTA)P_{10}-NH_2 (peptide **9**) with the conformation of a polyproline type II helix with the common dihedral angles of: ϕ = −75°, ψ = 145°, and ω = 180°. The calculated rotamer conformations are displayed via the opaque clouds.

Intracellular distance measurements on peptide 9. Distance measurements of peptide **9** were performed inside *Xenopus laevis* oocytes. The resulting DEER curve after background correction and the resulting distance distribution are shown in Figure 7 (for raw data and field sweep, see Figure S17−S19).

Model-free Tikhonov regularization reveals a bimodal distance distribution, featuring two maxima at 2.6 and 3.8 nm. The latter is in good accordance to the before mentioned distance distribution of peptide **9** in deuterated buffer (30 vol % glycerin-d_8), whereby the shape of the distribution at large distances above 3 nm is not accurate in this case due to the short analyzed dipolar evolution time.

The contribution at shorter distances around 2.6 nm suggests a partial conformational change to a PPI-helical conformation. PPI is a right-handed helix containing all cis peptide bonds and dihedral angles of ϕ = −75°, ψ = 160°, and ω = 0°, while the PPII helix is left-handed (dihedral angles: ϕ = −75°, ψ = 145°, and ω = 180°). The PPI helix is more compact than its left-handed counterpart, having a helical pitch of 5.6 Å with 3.3 residues per turn, whereas the PPII helix is extended, having a helical pitch of 9.3 Å and 3.0 residues per turn. The superposition of the results of the rotamer simulations of peptide **9** as a PPI and a PPII helix in a ratio of 10:9 describes the experimental distance distribution well (Figure 7, model of PPI helix shown in Figure 8).

The PPI helix is favored in environments with moderate dielectric constant, such as 1-propanol, whereas PPII helices dominate in aqueous solution[75−77] and polyprolines are known to be membrane permeable.[78,79] Therefore, our data suggest a localization of peptide **9** in the less polar environment of membranes and a corresponding conformational transition. In agreement with this point, the distance distribution obtained in an experiment with peptide **9** in cell extract after 1 h of incubation time (Figure S20)—featuring a low content of membrane fragments and no mitochondria at all[80]—shows no contribution at approximately 2.5 nm, as observed *in cellula* and features solely a distance distribution fitting with a PPII helical structure. Wennemers et al. showed that the length of an oligoproline and the type of its terminal groups influence the

dx.doi.org/10.1021/ja508274d | J. Am. Chem. Soc. 2014, 136, 15366−15378

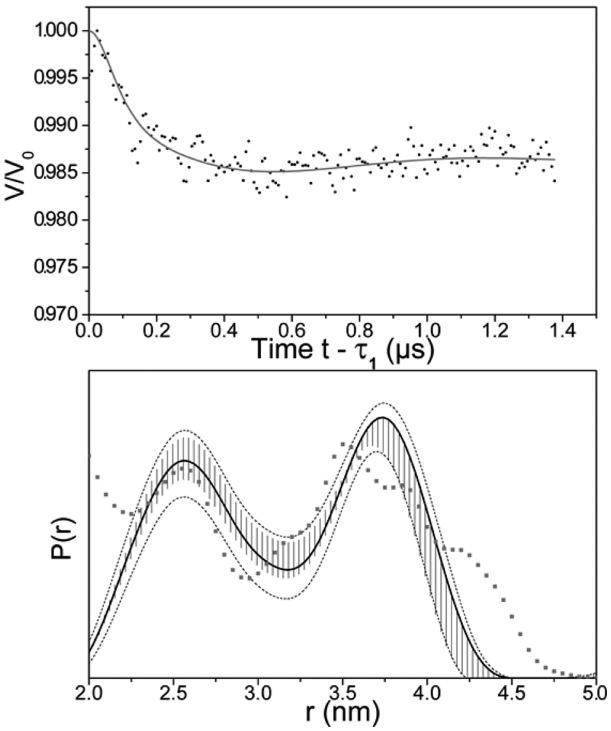

Figure 7. Top: Background corrected four-pulse DEER trace of peptide **9** inside *Xenopus laevis* oocytes after 1 h of incubation and Tikhonov regularization fit (black line) recorded at Q-band, 10 K; observer-pulses 16/16/32 ns, pump-pulse 16 ns, $\Delta\upsilon$ = 120 MHz, accumulation time 18 h. Bottom: Distance distribution obtained via Tikhonov regularization of the DEER trace (solid line). Calculated distance distribution for a right-handed PPI helix and a left-handed PPII helix in the ration of 10:9 (squares). The error bars are the full variation of the probability of given distances obtained during the statistical analysis (see Experimental Methods), whereas the dotted lines are upper/lower error estimations corresponding to the mean value ± two times the standard deviation of the different Tikhonov fits.

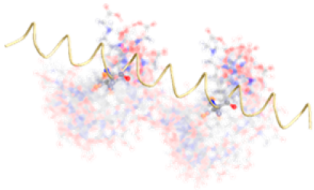

Figure 8. Model of H-$AP_{10}C$(Gd-PyMTA)$P_{10}C$(Gd-PyMTA)P_{10}-NH_2 (peptide **9**) with the conformation of a right-handed PPI helix. Chosen dihedral angles for modeling: ϕ = −75°, ψ = 160° and ω = 0°. The calculated rotamer conformations are displayed via the opaque clouds.

ratio of PPII and PPI.[81] The length of peptide **9** and the strongly polar and charged Gd-PyMTA labels may foster the PPI helix formation.

The distance distribution obtained for peptide **9** after an incubation time *in cellula* of only 5 min (see Figure S21) looks different than in buffer and different than after 1 h of incubation in cells. This supports the idea of a process on time scales of minutes or hours that involves a conformational change and an insertion into the membrane. Even though the conformational change is slow on the time scale of the EPR experiment, it is unusually fast for a PPII to PPI transition. To the best of our knowledge, such a fast conversion from PPII to PPI within 1 h (this was the incubation time used) has not been observed before. *In vitro* experiments with solvent exchange (from aqueous to aliphatic) revealed conversion times of days to weeks instead.[82,83] However, in virtually all cell types ranging from mammalian to bacteria,[84] peptidyl-prolyl cis−trans isomerases (PPIases) are found as enzymatic catalysts, which accelerate the slow cis−trans isomerization of the amide bonds in short oligopeptides[84−86] by several orders of magnitude.[87,88] This may explain our finding.

The assumption of a localization of peptide **9** in the cell membrane is supported by the intracellular DEER data revealing a local Gd(III) concentration of 2500 μM, which is more than 8 times higher than the overall concentration and still twice as high as the local Gd(III) concentration in the case of Gd-spacer-Gd (**10**) at the same overall concentration (see Table S1). This suggests an inhomogeneous distribution of the molecules in the cell, i.e. preferred compartments for localization of the peptide, as one would expect for the incorporation into membranes.[89]

Further important data obtained from the in-cell DEER measurements are signal-to-noise ratio and modulation depth λ. Both are lower for the intracellular DEER trace than those obtained in deuterated buffer. This is due to a 5.6 times shorter T_2 time of 1 μs in comparison to the measurement in deuterated buffer and the presence of the endogenous Mn(II) species.

Taking into account the contribution of in-cell Mn(II) species to the signal intensity at the observer frequency and the increase of the width of the Gd(III) spectrum in comparison to the spectral width of the measurement in deuterated buffer, a modulation depth λ_{corr} of 1.8% is estimated. The missing 0.7% when compared to the corresponding λ_{corr} in deuterated buffer can be assigned to rotamers of peptide **9** in the PPI conformation featuring distances below the lower limit of distances accessible by DEER (see Table S1). Hence, the experimental data is in full agreement with the assumption that the net modulation depth in *Xenopus oocytes* remains unchanged with respect to *in vitro* measurements and therefore suggests that the Gd-4-vinyl-PyMTA as well as its attachment to the peptide are stable *in cellula*.

SUMMARY AND CONCLUSIONS

With the current study, Gd(III) based site-directed spin labeling in combination with EPR distance measurements is shown to provide information on protein structures *in cellula*.

4-Vinyl-PyMTA (**3**) was used to attach Gd(III) to a peptide, extending the most common protocol for site-directed spin labeling, based on labeling the thiol group of the cysteine moiety. The selectivity of 4-vinyl-PyMTA (**3**) for cysteine was shown to be very high. Complete or nearly complete labeling of cysteine was achieved within 24 h at room temperature and 6 h at 40 °C, respectively, whereas the labeling of peptide **7** was surprisingly slow.

In terms of stability in the cellular environment, Gd-4-vinyl-PyMTA is superior compared to commonly used nitroxides. While the EPR signal of the latter decays with a half-life time of 85 min due to reduction to hydroxylamines, we found Gd-4-vinyl-PyMTA to be stable for at least 24 h in cell extract at 18 °C. In EPR distance measurements, the net modulation depth corresponding to the intramolecular Gd−Gd interaction of peptide **9** and Gd-spacer-Gd (**10**) is not reduced in *Xenopus oocytes* compared to *in vitro* measurements for at least 1 h. This indicates that not only the Gd-4-vinyl-PyMTA complex but also its attachment to the peptide is stable *in cellula*.

dx.doi.org/10.1021/ja508274d | J. Am. Chem. Soc. 2014, 136, 15366−15378

The EPR spectra of *Xenopus oocytes* contain an endogenous signal that can be ascribed to Mn(II) with an effective concentration of 10 μM. Two experiments indicate that accurate EPR distance measurements are feasible in the presence of the Mn(II) signal: (1) Mn(II)-DEER revealed that the Mn(II)-species are homogeneously distributed and therefore contribute to the background of a Gd(III)-DEER experiment, only. (2) DEER experiments using Gd-spacer-Gd (**10**) prove that distance determination *in cellula* works accurately in spite of the Mn(II) background.

With in-cell DEER in combination with Gd(III) based site-directed spin labeling, we have shown a localization of the proline rich peptide **9**, H-AP$_{10}$C(Gd-PyMTA)P$_{10}$C(Gd-PyMTA)P$_{10}$-NH$_2$, within the cell, suggesting an incorporation into membranes. Furthermore, this peptide undergoes a partial conformational transition from a PPII helix into a PPI helix. Control experiments in cell extract under indentical incubation conditions did not show this transition. The experimental distance distributions agree with data for peptide **9** in the conformation of a PPI and a PPII helix that were obtained through simulation on the basis of a rotamer library of a cysteine attached Gd-PyMTA, taking the flexibility of the tether into account.

EXPERIMENTAL METHODS

General. Potassium vinyltrifluoroborate (>97%, TCI), Cs_2CO_3 (>98%, Fluka), tris(hydroxymethyl)aminomethane ($H_2NC(CH_2OH)_3$, Tris; ≥97%, Sigma), trifluoroacetic acid (Solvay Fluor), tris(2-carboxyethyl)phosphine·HCl (TCEP·HCl; 98%, Acros), L-alanine (Degussa), L-arginine (>97%, Fluka), L-cysteine (>97%, Acros), L-histidine (>99%, Serva), L-lysine·H_2O (≥98%, Aldrich), L-proline (>99%, Fluka), peptide (H-AP$_{10}$CP$_{10}$CP$_{10}$-NH$_2$) (ca. 90%, contains a small amount of M ± proline, Biosyntan), phosphoric acid (≥85 wt %, Sigma-Aldrich), $GdCl_3$·6H_2O (99.999% trace metals basis, Aldrich), EtOH (absolute, AnalaR, VWR), MeCN (HPLC, VWR), acetone (AnalaR, VWR), and 3-carboxy-2,2,5,5-tetramethyl-1-pyrrolidinyloxy (3-carboxy-PROXYL, Sigma-Aldrich) were used as received. $PdCl_2(PPh_3)_2$[90] was synthesized according to the literature. THF (HPLC, VWR) was distilled from sodium/benzophenone. For the preparation of the aqueous solutions, deionized water was used.

The proton-exchange resin (Dowex 50WX4 hydrogen form, Sigma-Aldrich, 91 g) was subsequently washed with THF (3 × 200 mL), EtOH (2 × 100 mL), H_2O (2 × 150 mL), and EtOH (200 mL) and dried over P_2O_5 at 0.05 mbar for 5 days to obtain a pure and dry proton-exchange resin (30 g).

Column chromatography was carried out on silica gel 60 M (Acros) applying slight pressure. In the preparation procedure below, the size of the column is given as diameter × length. Thin layer chromatography was performed on silica gel coated aluminum foil (Merck, 60 F254). The spots were detected with UV light of λ = 254 nm. The compositions of solvent mixtures are given in volume ratios.

Preparation of Tris-HCl buffer (pH 8.0, 0.05 M): We followed a procedure given in ref 91. An aqueous solution of tris(hydroxymethyl)aminomethane (Tris) (50 mL, 0.1 M) and HCl (29.2 mL, 0.1 M) was mixed and diluted to 100 mL. pH indicator strips (resolution: 0.2 pH, Merck) were used to determine the pH of the solution.

NMR spectra were calibrated using the solvent signal as an internal standard [$CDCl_3$: $\delta(^1H)$ = 7.25, $\delta(^{13}C)$ = 77.0; D_2O: $\delta(^1H)$ = 4.79] For ^{13}C NMR experiments in D_2O a drop of MeOH was added as the internal standard [$\delta(^{13}C)_{MeOH}$ = 49.5]. In the case of ^{31}P NMR spectra a closed capillary filled with phosphoric acid in D_2O (0.25 M) served for the field lock and the signal of phosphoric acid in D_2O [$\delta(^{31}P)$ = 0] was used for calibration. For the samples in Tris-HCl buffer, the signal of Tris ($\delta(^1H)$ = 3.52) was used as an internal standard and the ^1H NMR spectra were measured using water-suppression by a presaturation technique.[67] In these cases, a closed capillary (80 mm × 1.5 mm) with D_2O was used for the field lock. Signal assignment is supported by DEPT-135, COSY, HMBC, and HMQC experiments.

ESI MS spectra were recorded using an Esquire 3000 ion trap mass spectrometer (Bruker Daltonik) equipped with a standard ESI source. Accurate MS experiments were performed using a Fourier transform ion cyclotron resonance (FT-ICR) mass spectrometer APEX III (Bruker Daltonik) interfaced to an external ESI ion source.

4-Vinyl-PyMTA tetraethyl ester (2). This reaction was performed under argon. A solution of 4-iodo-PyMTA (**1**) (1.00 g, 1.65 mmol), potassium vinyltrifluoroborate (441 mg, 3.29 mmol), and Cs_2CO_3 (2.15 g, 6.59 mmol) in THF (30 mL) and H_2O (4.5 mL) was degassed through three freeze−pump−thaw cycles. $PdCl_2(PPh_3)_2$ (58 mg, 82.6 μmol) was added. The solution was refluxed at 85 °C for 16 h. The solvents were removed using a rotary evaporator (40 °C, reduced pressure). Column chromatography (5 cm × 25 cm, pentane/Et_2O 1:2) gave a pale yellow oil (688 mg) consisting of 4-vinyl-PyMTA tetraethyl ester (**2**) (82% yield) and a trace of an unidentified organic compound (about 2 mol %). ^1H NMR (500 MHz, $CDCl_3$): Signals assigned to 4-vinyl-PyMTA tetraethyl ester (**2**): δ = 7.43 (s, 2H, ArH), 6.62 (dd, ^3J = 17.6 and 10.9 Hz, 1H, ArCH), 5.95 (d, ^3J = 17.6 Hz, 1H, ArCH=C$\underline{H}_{cis}H_{trans}$), 5.39 (d, ^3J = 10.9 Hz, 1H, ArCH=CH$_{cis}\underline{H}_{trans}$), 4.10 (q, ^3J = 7.1 Hz, 8H, C$\underline{H}_2$CH$_3$), 3.97 (s, 4H, ArC$\underline{H}_2$), 3.55 (s, 8H, C$\underline{H}_2$CO$_2$Et), 1.20 (t, ^3J = 7.1 Hz, 12H, CH$_3$); additional signals of very low intensity (Figure S8b): δ = 7.24 (s, 2H), 5.74 (m, 1H), 4.95 (dq, J = 17.1 Hz, 1.6 Hz, 1H), 4.90 (dd, J = 10.3 Hz, 1.2 Hz, 1H), 3.95 (s, 4H), 3.54 (s, 8H), 2.64 (t, J = 7.5 Hz, 2H), 2.31 (q, J = 7.5 Hz, 2H). ^{13}C NMR (125 MHz, $CDCl_3$): δ = 171.0 (C=O), 158.6 (C_{Ar} *meta* to vinyl), 146.0 ($\underline{C}_{Ar}$-CH=CH$_2$), 135.1(C_{Ar}-$\underline{C}$H=CH$_2$), 118.4 (C_{Ar}-CH=$\underline{C}$H$_2$), 118.3 (C_{Ar}H), 60.4 ($\underline{C}$H$_2$CH$_3$), 59.8 (ArCH$_2$), 54.8 ($\underline{C}$H$_2$CO$_2$Et), 14.1 (CH$_3$). MS (ESI): m/z = 530.4 [M + Na]$^+$, 508.5 [M + H]$^+$. Elemental analysis calcd (%) for $C_{25}H_{37}N_3O_8$ (507.577): C, 59.16; H, 7.35; N, 8.28; O, 25.22. Found C, 58.74; H, 7.71; N, 8.25. Accurate MS (ESI): calcd. for [M + Na]$^+$ $C_{25}H_{37}N_3O_8$Na: 530.24729; found 530.24614.

4-Vinyl-PyMTA (3) (ester hydrolysis product). The published procedure[64] was followed, making small changes. Water (2 mL) and then NaOH aqueous solution (2 M, 1.74 mL, 3.48 mmol) were added to a solution of 4-vinyl-PyMTA ester **2** (353 mg, 695 μmol) in EtOH (2 mL), whereupon a mixture of two liquid phases formed. During 10 min of stirring at room temperature, the reaction mixture became a pale yellow one phase solution. This was stirred for another 24 h. Then proton-exchange resin was added as much as was needed to reduce the pH of the solution to ca. 3. The solution was separated from the proton-exchange resin through filtration, and the ion-exchange resin was washed three times with a 1:1 mixture of EtOH and H_2O (6 mL). The solvents of the combined filtrates were removed using a rotary evaporator (40 °C, reduced pressure). The pale brown viscous residue was dissolved in H_2O (2 mL), and the solution was dropped into acetone (15 mL) under stirring, giving an emulsion. Centrifugation of this emulsion at 13400 rpm in an Eppendorf MiniSpin (6 cm rotor radius) for 2 min separated the mixture into two phases: a pale brown oil and a colorless liquid. The colorless liquid was removed with the help of a pipet, and the pale brown oil was dried over P_2O_5 at 0.05 mbar for 16 h. A pale brown solid (255 mg) was obtained, containing ca. 90 wt % of 4-vinyl-PyMTA (**3**) (83% yield), a trace of unidentified organic compound, and ca. 10 wt % of inorganic matter. ^1H NMR (500 MHz, D_2O): Signals assigned to 4-vinyl-PyMTA (**3**): δ = 7.57 (s, 2H, ArH), 6.78 (dd, ^3J = 17.6 and 10.9 Hz, 1H, ArCH), 6.16 (d, ^3J = 17.6 Hz, 1H, ArCH=C$\underline{H}_{cis}H_{trans}$), 5.65 (d, ^3J = 10.9 Hz, 1H, ArCH=CH$_{cis}\underline{H}_{trans}$), 4.67 (s, 4H, ArC$\underline{H}_2$), 3.99 (s, 8H, C$\underline{H}_2CO_2$H); additional signals of very low intensity (Figure S10,b): δ = 7.41 (s, 2H), 5.83 (m, 1H), 4.99 (m, 1H), 4.96 (br s, 1H), 4.64 (s, 4H), 3.96 (s, 8H), 2.82 (t, J = 7.5 Hz, 2H), 2.41 (q, J = 7.5 Hz, 2H). ^{13}C NMR (125 MHz, D_2O): δ = 170.5 (C=O), 150.8 (C_{Ar} *meta* to vinyl), 149.2 ($\underline{C}_{Ar}$-CH=CH$_2$), 133.9 (C_{Ar}-$\underline{C}$H=CH$_2$), 122.7 (C_{Ar}H) 122.2 (C_{Ar}-CH=$\underline{C}$H$_2$), 59.0 (ArCH$_2$), 57.3 ($\underline{C}$H$_2$CO$_2$H). MS (ESI): m/z = 418.2 [M + Na]$^+$, 396.3 [M + H]$^+$. Elemental analysis calcd (%) for $C_{17}H_{21}N_3O_8$ (395.364): C, 51.64; H, 5.35; N, 10.63; O, 32.37. Found C, 47.32; H, 4.73; N, 9.53. Accurate MS (ESI): calcd. for [M + H]$^+$ $C_{17}H_{21}N_3O_8$H: 396.14014; found 396.13900.

dx.doi.org/10.1021/ja508274d | J. Am. Chem. Soc. 2014, 136, 15366−15378

Gd-4-vinyl-PyMTA (4). An aqueous solution of $GdCl_3$ (0.1 M; 1670 μL, 167 μmol) was added to a solution of 4-vinyl-PyMTA (**3**) (73.5 mg of ester hydrolysis product; this corresponds to 167 μmol of 4-vinyl-PyMTA) in H_2O (2 mL). Aqueous NaOH solution (0.01 M) was added as much as was needed to raise the pH of the solution to 7.2. The solution was diluted to 6.680 mL to obtain a solution of Gd(III)-4-vinyl-PyMTA (**4**) (25 mM). MS (ESI): m/z = 548.9 $[M - Na]^-$. Accurate MS (ESI): calculated for $[M + Na]^+$. $C_{17}H_{17}GdN_3NaO_8Na^+$: 595.00466; found 595.00463 (Figure S12).

Ligand carrying peptide 8. This reaction was performed under argon. Peptide **7** (11.1 mg, 3.46 μmol) and 4-vinyl-PyMTA (**3**) (ester hydrolysis product 13.6 mg corresponding to 30.9 μmol of 4-vinyl-PyMTA) were dissolved in Tris-HCl buffer (25 mM, pH 8.0; 3 mL). The pH of the colorless solution was 7.8. The solution was degassed through three freeze−pump−thaw cycles and heated to 40 °C. The reaction was monitored by HPLC-MS. Allover 100 μL of the reaction mixture was removed for this monitoring. After 80 h the reaction was complete. The reaction solution was concentrated to ca. 1 mL through freeze-drying. Ligand carrying peptide **8** was isolated by HPLC on a C18(2) column (5 μm, 100 Å, 21.2 mm × 250 mm, Luna Phenomenex) by applying a linear gradient elution with a flow rate of 12 mL/min at room temperature and UV detection at 220 nm. The mobile phase consisted of A (H_2O/MeCN/TFA, 95:5:0.1, v/v/v) and B (MeCN/H_2O/TFA, 95:5:0.1, v/v/v) with the following percentages of B: 0−5 min, 0%; 5−25 min, 0%−60%; 25−30 min, 60%. The eluate between 21 and 24 min was collected and freeze-dried to give ligand carrying peptide **7** (12.2 mg, 88%) as a colorless solid. MS (ESI): m/z = 2016.0 $[M - 3H + K]^{2-}$, 2008.0 $[M - 3H + Na]^{2-}$, 1997.1 $[M - 2H]^{2-}$, 1356.6 $[M - 5H + 2K]^{3-}$, 1351.3 $[M - 5H + Na + K]^{3-}$. Accurate MS (ESI): calcd. for $[M - 3H]^{3-}$ $C_{193}H_{267}N_{40}O_{49}S_2$: 1330.96962; found 1330.97043.

Spin labeled peptide 9. An aqueous solution of $GdCl_3$ (0.01 M; 458 μL, 4.58 μmol) was added to the solution of ligand carrying peptide **8** (9.4 mg, 2.35 μmol) in H_2O (3 mL). Aqueous NaOH solution (0.01 M; 3250 μL, 32.5 μmol) was added to the colorless solution to raise the pH to ca. 7.2. Through freeze-drying, a colorless solid (10.9 mg) consisting of spin labeled peptide **9** and sodium chloride was obtained. MS (ESI): m/z = 2152.1 $[M - 2Na]^{2-}$, 2103.1 $[M - pro - 2Na]^{2-}$, 2200.6 $[M + pro - 2Na]^{2-}$. Accurate MS (ESI): calculated for $[M - 2Na]^{2-}$ $C_{193}H_{262}Gd_2N_{40}O_{49}S_2$: 2151.85869; found 2151.85345 (Figure S13).

The reaction between 4-vinyl-PyMTA (3) and TCEP. The reaction was performed in an NMR tube. 4-Vinyl-PyMTA (**3**) (12.1 mg of ester hydrolysis product; this corresponds to 27.5 μmol of 4-vinyl-PyMTA), and TCEP·HCl (8.9 mg, 31.1 μmol) were dissolved in Tris-HCl buffer (pH 8.0, 0.05 M; 0.6 mL). The pH of the solution was adjusted to 7.8 through the addition of Tris. The solution stood at room temperature for 20 h, and then NMR and MS spectra were recorded. ^{1}H NMR (500 MHz, Tris-HCl buffer, Figure S1,b): Signals assigned to TCEP adduct **5**: δ = 7.33 (s, 2H, ArH), 4.40 (s, 4H, $ArCH_2N$), 3.66 (s, 8H, $NC\underline{H}_2CO_2H$), 2.91 (m, 2H, $ArC\underline{H}_2CH_2$), 2.49 (m, 2H, $ArCH_2C\underline{H}_2$), 2.38 (m, 12H, $PC\underline{H}_2C\underline{H}_2CO_2H$). Signals assigned to TCEP-oxide: δ = 2.24 (m, 6H, $PCH_2C\underline{H}_2CO_2H$), 1.94 (m, 6H, $PC\underline{H}_2CH_2CO_2H$). The additional broad and unstructured signal of low intensity at 2.29 ppm may be due to TCEP. ^{31}P NMR (200 MHz, Tris-HCl buffer): δ = 58.7 (TCEP-oxide), 35.6 (TCEP adduct **5**). MS (ESI) m/z = 646.3 $[\mathbf{5} - Cl]^+$, 668.2 $[\mathbf{5} - H + Na - Cl]^+$, 690.2 $[\mathbf{5} - 2H + 2Na - Cl]^+$.

Competition of cysteine and TCEP for 4-vinyl-PyMTA (3). The reaction was performed in an NMR tube. 4-Vinyl-PyMTA (**3**) (12.3 mg of ester hydrolysis product; this corresponds to 28.0 μmol of 4-vinyl-PyMTA), cysteine (3.4 mg, 28.1 μmol), and TCEP·HCl (7.9 mg, 27.6 μmol) were dissolved in Tris-HCl buffer (pH 8.0, 0.05 M; 0.6 mL). The pH of the solution was adjusted to 7.8 through the addition of Tris. The reaction solution stood at room temperature for 18 h. ^{1}H NMR spectroscopy revealed a 57:43 mixture of TCEP adduct **5** and cysteine adduct **6**. ^{1}H NMR (500 MHz, Tris-HCl buffer, Figure S1,c): Signals assigned to TCEP adduct **5**: δ = 7.31 (s, 2H, ArH), 4.44 (s, 4H, $ArCH_2N$), 3.69 (s, 8H, $NC\underline{H}_2CO_2H$), 2.90 (m, 2H, $ArC\underline{H}_2CH_2$, overlapping with the signal of cysteine adduct **6** and cysteine), 2.46 (m, 2H, $ArCH_2C\underline{H}_2$), and 2.36 (m, 12H, $PC\underline{H}_2C\underline{H}_2CO_2H$). Signals assigned to cysteine adduct **6**: δ = 7.28 (s, 2H, ArH), 4.40 (s, 4H, $ArCH_2N$), 3.72 (dd, ^3J = 7.2 Hz, 4.3 Hz, 1H, $C\underline{H}NH_2$), 3.67 (s, 8H, $NC\underline{H}_2CO_2H$), 2.95−2.70 (m, 6H, $ArC\underline{H}_2C\underline{H}_2$ and CH_2S, overlapping with the signal of TCEP adduct **5** and cysteine). Signals assigned to TCEP-oxide: δ = 2.21 (m, 6H, $PCH_2C\underline{H}_2CO_2H$), 1.92 (m, 6H, $PC\underline{H}_2CH_2CO_2H$). Signals assigned to TCEP: δ = 2.29 (broad signal overlapping with the signal of TCEP-adduct **5**, 6H, $PCH_2C\underline{H}_2CO_2H$), 2.05 (very broad and unstructured, 6H, $PC\underline{H}_2CH_2CO_2H$). Signals assigned to cysteine: δ = 3.77 (dd, ^3J = 5.8 Hz, 4.2 Hz, 1H, $C\underline{H}NH_2$), 2.95−2.70 (m, 2H, CH_2S, overlapping with the signal of TCEP adduct **5** and cysteine adduct **6**). ^{31}P NMR (200 MHz, Tris-HCl buffer): δ = 58.7 (TCEP-oxide), 52.6 (very low intensity; unknown origin), 35.6 (TCEP adduct **5**).

Preparation of the *Xenopus laevis* oocytes extract (CSF). The *Xenopus* cytostatic factor arrested (CSF) oocyte extract was prepared essentially as described by Murray.[92] Briefly: Female frogs were primed by injection with 150 IU of pregnant mare serum gonadotropin. For ovulation, female frogs were transferred to MMR medium and injected with 300 IU of human chorionic gonadotropin. Following induced ovulation, oocytes were sorted and washed with MMR medium. Subsequent to dejellying in dejellying solution (2% (w/v) cysteine in 1 × XB salts (100 mM KCl, 0.1 mM $CaCl_2$, 1 mM $MgCl_2$, pH 7.8) and three washing steps (CSF-XB (1× XB salts, 50 mM sucrose, 10 mM potassium HEPES (2-[4-(2-hydroxyethyl)piperazin-1-yl]-ethanesulfonic acid), 5 mM EDTA, pH 7.7)), activated (dividing) and lysed oocytes were removed and intact oocytes retained. Intact oocytes were then transferred to a centrifugation tube prefilled with CSF-XB and cytochalasin B. After an initial centrifugation step (2 min, 1000 rpm, 4 °C) and removal of supernatant, oocytes were lysed by a second centrifugation (20 min, 10000 rpm, 4 °C). CSF was extracted with a syringe from the middle yellowish layer in the centrifugation tube. To control for the integrity of the CSF extract, spindle morphology was observed following addition of $CaCl_2$ and sperm nuclei to an aliquot of the CFS extract.[93] The obtained oocyte extract was frozen with liquid nitrogen and stored at −80 °C until further use (it was taken from the freezer and thawed immediately prior to sample preparation).

Sample preparation for EPR measurements. Gd-spacer-Gd (**10**) and peptide **9** were dissolved in D_2O and 10 mM Tris-HCl buffer (D_2O, pH 7.4), respectively, and mixed with glycerin-d_8, resulting in a final concentration of 200 μM (30 vol % glycerin-d_8). Each sample was collected in a Q-band test tube (quartz glass 1 mm inner diameter, purchased from BRUKER Bospin), immediately shock-frozen in liquid nitrogen, and stored at −80 °C until further use.

Preparation and microinjection of *Xenopus laevis* oocytes. The *Xenopus laevis* oocytes on stage V/VI (purchased from EcoCyte Bioscience, Caustrop-Rauxel, Germany) were kept in MBS (modified Barth's saline, 1×: 88 mM NaCl, 1 mM KCl, 1 mM $MgSO_4$, 5 mM HEPES (2-[4-(2-hydroxyethyl)piperazin-1-yl]ethanesulfonic acid), 2.5 mM $NaHCO_3$, 0.7 mM $CaCl_2 \cdot H_2O$) at 18 °C. Prior to the microinjection, six oocytes were prepared on a self-made poly-(tetrafluoroethylene) holder in MBS (1×) and visually inspected. 50 nL of a solution of Gd-spacer-Gd (**10**) in H_2O or of a solution of peptide **9** in Tris-HCl buffer (pH 7.4) with a concentration of 8 mM was microinjected into the oocytes, using a Nanoject II automatic nanoliter injector with fitting micromanipulator MM33 (DRUMMOND). Afterward, the oocytes were washed carefully with MBS (1×). Three of them were then collected cautiously in a Q-band tube (quartz glass, 1 mm inner diameter, purchased from BRUKER Biospin) via slightly negative pressure on one end of the tube. The oocytes were visually inspected directly afterward as well as after the incubation time using a Stemi 2000-C binocular microscope mounted with an AxiaCam ERc 5s camera (ZEISS), and—after removal of supernatant MBS—shock-frozen in liquid nitrogen. The samples were kept at −80 °C until measuring them without defreezing.

For measurements of untreated *Xenopus laevis* oocytes, the oocytes were shock-frozen in liquid nitrogen. Afterward, they were crushed on a metal plate cooled with dry ice and filled in a Q-band sample tube (closed at one side, quartz glass, 1 mm inner diameter, purchased from

BRUKER Biospin). The oocytes were then transferred into a Q-band tube without unfreezing them. The filled Q-band test tube was sealed and stored at −80 °C.

EPR measurements. Q-band EPR experiments were performed at 34 GHz microwave frequency using an ELEXSYS E500 spectrometer equipped with an EN 5107D2 Q-band EPR probe head (both Bruker Biospin) and a 10 W MW power solid state amplifier (HBH Microwave GmbH). A CF935 helium gas flow system (Oxford Instruments) was used for temperature control.

Two pulse echo-detected field sweeps were obtained at T = 10 K using a Hahn-echo sequence with τ = 400 ns, $\pi/2$ pulse = 8 ns, and π pulse =16 ns and a sweep width of 4000 G with B_0 = ∼12200 G.

T_2 relaxation time experiments were performed via a Hahn-echo sequence with pulse lengths of 8 and 16 ns for $\pi/2$ and π pulse, respectively. The time separation τ between pulses was increased from 400 to 16000 ns in 4 ns steps. The relaxation time was determined from the exponential fit of the acquired decay.

The four-pulse, dead-time-free DEER was obtained using the following pulse sequence:

$$\left(\frac{\pi}{2}\right)_{obs}\cdots\tau_1\cdots(\pi)_{pump}\cdots(\tau_1+\tau_2-t)\cdots(\pi)_{obs}\cdots\tau_2\cdots echo$$

The pump pulse (length 16 ns) was set to the maximum of the Gd(III) spectrum, and the observer pulses (lengths 16/16/32 ns) were shifted 120 MHz (if not mentioned otherwise) to lower frequencies. The time separation τ_1 was 400 ns, and the corresponding dipolar evolution time τ_2 can be obtained from the corresponding figure. Shot repetition time was set to 2 ms. Accumulation time per sample is indicated in the corresponding figure.

Nuclear modulation artifacts of matrix deuterons of D_2O and deuterated buffer, respectively, were suppressed by variation of the interpulse delay τ_1, adding traces of eight values with $\Delta\tau_1$ = 16 ns.[15,26]

Stability of Gd-4-vinyl-PyMTA (4) and of 3-carboxy-PROXYL in cell extract determined by EPR. Time-dependent EPR measurements of Gd-4-vinyl-PyMTA (**4**) and 3-carboxy-PROXYL were performed in *Xenopus laevis* cell extract (CSF). The corresponding sample was mixed with cell extract in a ratio of 1:3 (vol./vol.) to receive 20 μL of the sample solution with a final spin concentration of 500 μM. The solution was vortexed for 30 s and loaded into a glass capillary (outer diameter 1 mm) with a sample volume of 20 μL. Measurements were performed at X-band using a MS200 miniscope spectrometer (Magnettech GmbH) equipped with a TCH02 temperature controller (Magnettech GmbH) at T = 18 °C. The spectra of the Gd-4-vinyl-PyMTA (3-carboxy-PROXYL) were obtained with a modulation amplitude of 7 G (0.6 G), a microwave attenuation of 4 dB (24 dB), and a sweep width of 2000 G (80 G) with a sweep time of 160 s (43 s). The signal intensity of the measurement was given by the signal amplitude of the (central) peak.

Generation of the rotamer library. An initial model of the ligand complexed with Gd^{3+} and attached to cysteine was generated with ChemBioDraw and ChemBio3D 12 (Cambridge Soft) and geometry optimized with ORCA[94] using the B3LYP density functional with SVP basis sets for all atoms and the zeroth-order regular approximation for relativistic effects. All programs for the following steps were home-written in Matlab. To generate an ensemble of 20,000 low-energy conformations, dihedral angles of all rotatable bonds of the linker were varied by a Monte Carlo approach, using UFF force field parameters[73] for torsion and nonbonding energy potentials. The UFF force field file was taken from the Towhee implementation.[95] Variation of bond lengths, bond angles, and electrostatic interactions was neglected. Conformations were accepted if their Boltzmann population at ambient temperature was at least 1% of the population of the lowest-energy conformation encountered in a prerun with 10,000,000 Monte Carlo trials.

The 20,000 low-energy conformations were hierarchically clustered in dihedral angle space, using a cyclic metric. A number of 324 rotamers arise from the multiplicity of the torsion potentials of the rotatable bonds, in agreement with distributions of the corresponding dihedral angles for the ensemble. Relative rotamer populations were computed from the Boltzmann populations of the individual conformations. For attachment to the peptide, relative energies resulting from Bolzmann inversion of these populations were augmented by the interaction energy with the peptide as described before,[61] assuming UFF nonbonding potentials and a forgive factor of 0.50 that was optimized against experimental data with a library of the methanethiosulfonato spin label that had been obtained analogously. Detailed description, discussion, and validation of this new approach to rotamer library generation will be published elsewhere.

EPR data analysis. The DEER curves were analyzed using the DeerAnalysis2013.2 software package for MATLAB.[72] Distance distributions obtained from Tikhonov regularizations were validated using the validation tool of DeerAnalysis2013.2. For this, 160 regularizations were performed, gradually changing the parameter background start and adding white noise to receive an error estimate of the corresponding distribution and an appropriate background starting point. The error bars are the full variation of the probability of given distances, whereas the dotted lines are upper/lower error estimations corresponding to the mean value ± two times the standard deviation of the different Tikhonov fits.

MMM (multiscale modeling of macromolecular systems) was used to calculate the distance distribution of the modeled polyproline helices.[61] The models of polyproline helix type I and type II were designed with the UCSF Chimera package.[96]

Spin concentrations of in-cell measurements were determined using as reference the echo-detected field sweeps of Gd-spacer-Gd (**10**) and spin labeled peptide **9** in D_2O and deuterated buffer, respectively, with 30 vol % glycerin-d_8 at Q-band (T = 10 K). Through superposition of these spectra with the independently measured spectrum of $MnCl_2$ in D_2O with 30 vol % of glycerin-d_8 (same conditions and pulses as the above-mentioned measurements), the ratio of the two components in the experimental data of the corresponding in-cell measurements was determined. The obtained ratio was used to estimate the concentration of the particular spin species inside the cell (Figure S14, Table S1).

■ ASSOCIATED CONTENT

Ⓢ Supporting Information

Additional EPR data, NMR spectra, ESI-MS spectra, and calculations regarding EPR data analysis. This material is available free of charge via the Internet at http://pubs.acs.org.

■ AUTHOR INFORMATION

Corresponding Authors

godt@uni-bielefeld.de
malte.drescher@uni.kn

Author Contributions

‖M. Qi and A. Gro contributed equally.

Notes

The authors declare no competing financial interest.

■ ACKNOWLEDGMENTS

This work was supported by the Deutsche Forschungsgemeinschaft within SPP 1601 and by a grant from the Ministry of Science, Research and the Arts of Baden-Württemberg (AZ: 33-7532.20/723). A.G. is thankful for the funding of a sabbatical stay at the University of Konstanz and thus the fostering of this collaborative research through the Zukunftskolleg of the University of Konstanz.

■ REFERENCES

(1) Serber, Z.; Corsini, L.; Durst, F.; Dötsch, V. In *Methods in Enzymology*; Thomas, L. J., Ed.; Academic Press: Burlington, 2005; Vol. *394*, p 17.

(2) Hubbard, J. A.; MacLachlan, L. K.; King, G. W.; Jones, J. J.; Fosberry, A. P. *Mol. Microbiol.* **2003**, *49*, 1191.

(3) Dedmon, M. M.; Patel, C. N.; Young, G. B.; Pielak, G. J. *Proc. Natl. Acad. Sci. U. S. A.* **2002**, *99*, 12681.
(4) Wieruszeski, J. M.; Bohin, A.; Bohin, J. P.; Lippens, G. *J. Magn. Reson.* **2001**, *151*, 118.
(5) Serber, Z.; Keatinge-Clay, A. T.; Ledwidge, R.; Kelly, A. E.; Miller, S. M.; Dötsch, V. *J. Am. Chem. Soc.* **2001**, *123*, 2446.
(6) Serber, Z.; Ledwidge, R.; Miller, S. M.; Dötsch, V. *J. Am. Chem. Soc.* **2001**, *123*, 8895.
(7) Sakai, T.; Tochio, H.; Tenno, T.; Ito, Y.; Kokubo, T.; Hiroaki, H.; Shirakawa, M. *J. Biomol. NMR* **2006**, *36*, 179.
(8) Selenko, P.; Serber, Z.; Gadea, B.; Ruderman, J.; Wagner, G. *Proc. Natl. Acad. Sci. U. S. A.* **2006**, *103*, 11904.
(9) Serber, Z.; Selenko, P.; Hansel, R.; Reckel, S.; Lohr, F.; Ferrell, J. E.; Wagner, G.; Dotsch, V. *Nat. Protoc.* **2007**, *1*, 2701.
(10) Miyawaki, A.; Llopis, J.; Heim, R.; McCaffery, J. M.; Adams, J. A.; Ikura, M.; Tsien, R. Y. *Nature* **1997**, *388*, 882.
(11) Hänsel, R.; Luh, L. M.; Corbeski, I.; Trantirek, L.; Dötsch, V. *Angew. Chem., Int. Ed.* **2014**, *53*, 2.
(12) Schiemann, O.; Piton, N.; Plackmeyer, J.; Bode, B. E.; Prisner, T. F.; Engels, J. W. *Nat. Protoc.* **2007**, *2*, 904.
(13) Hubbell, W. L.; Cafiso, D. S.; Altenbach, C. *Nat. Struct. Mol. Biol.* **2000**, *7*, 735.
(14) Altenbach, C.; Marti, T.; Khorana, H.; Hubbell, W. *Science* **1990**, *248*, 1088.
(15) Jeschke, G.; Pannier, M.; Godt, A.; Spiess, H. W. *Chem. Phys. Lett.* **2000**, *331*, 243.
(16) Jeschke, G. *Annu. Rev. Phys. Chem.* **2012**, *63*, 419.
(17) Milov, A. D.; Salikhov, K. M.; Shchirov, M. D. *Fizika Tverdogo Tela* **1981**, *23*, 975.
(18) Yu, D. T.; Milov, A. D.; Maryasov, A. G. *Russ. Chem. Rev.* **2008**, *77*, 487.
(19) Martin, R. E.; Pannier, M.; Diederich, F.; Gramlich, V.; Hubrich, M.; Spiess, H. W. *Angew. Chem., Int. Ed.* **1998**, *37*, 2833.
(20) Jeschke, G.; Sajid, M.; Schulte, M.; Ramezanian, N.; Volkov, A.; Zimmermann, H.; Godt, A. *J. Am. Chem. Soc.* **2010**, *132*, 10107.
(21) Hubbell, W. L.; Altenbach, C. *Curr. Opin. Struct. Biol.* **1994**, *4*, 566.
(22) Constantine, K. L. *Biophys. J.* **2001**, *81*, 1275.
(23) Jeschke, G.; Polyhach, Y. *Phys. Chem. Chem. Phys.* **2007**, *9*, 1895.
(24) Steinhoff, H.-J.; Suess, B. *Methods* **2003**, *29*, 188.
(25) Rabenstein, M. D.; Shin, Y. K. *Proc. Natl. Acad. Sci. U. S. A.* **1995**, *92*, 8239.
(26) Jeschke, G.; Bender, A.; Paulsen, H.; Zimmermann, H.; Godt, A. *J. Magn. Reson.* **2004**, *169*, 1.
(27) Borbat, P. P.; Davis, J. H.; Butcher, S. E.; Freed, J. H. *J. Am. Chem. Soc.* **2011**, *126*, 7746.
(28) Eaton, S.; Eaton, G. In *Distance Measurements in Biological Systems by EPR*; Berliner, L. J., Eaton, G. R., Eaton, S. S., Eds.; Springer: New York, NY, 2002; Vol. *19*, p 1.
(29) Drescher, M. In *EPR Spectroscopy*; Drescher, M., Jeschke, G., Eds.; Springer: Berlin, Heidelberg, 2012; Vol. *321*, p 91.
(30) Ward, R.; Bowman, A.; Sozudogru, E.; El-Mkami, H.; Owen-Hughes, T.; Norman, D. G. *J. Magn. Reson.* **2010**, *207*, 164.
(31) Jeschke, G. *ChemPhysChem* **2002**, *3*, 927.
(32) Banham, J. E.; Timmel, C. R.; Abbott, R. J. M.; Lea, S. M.; Jeschke, G. *Angew. Chem., Int. Ed.* **2006**, *45*, 1058.
(33) Godt, A.; Schulte, M.; Zimmermann, H.; Jeschke, G. *Angew. Chem., Int. Ed.* **2006**, *45*, 7560.
(34) Jeschke, G.; Spiess, H. W. In *Novel NMR and EPR Techniques*; Dolinsek, J., Vilfan, M., Zumer, S., Beig, R., Beiglböck, W., Domcke, W., Englert, G., Frisch, U., Hänggi, P., Hasinger, G., Hepp, K., Hillebrandt, W., Imboden, D., Jaffe, R. L., Lipowsky, R., Löhneysen, H. v., Ojima, I., Sornette, D., Theisen, S., Weise, W., Wess, J., Zittartz, J., Eds.; Springer: Berlin, 2006; Vol. *684*, p 21.
(35) Azarkh, M.; Okle, O.; Singh, V.; Seemann, I. T.; Hartig, J. S.; Dietrich, D. R.; Drescher, M. *ChemBioChem* **2011**, *12*, 1992.
(36) Azarkh, M.; Singh, V.; Okle, O.; Seemann, I. T.; Dietrich, D. R.; Hartig, J. S.; Drescher, M. *Nat. Protoc.* **2013**, *8*, 131.
(37) Krstić, I.; Hänsel, R.; Romainczyk, O.; Engels, J. W.; Dötsch, V.; Prisner, T. F. *Angew. Chem., Int. Ed.* **2011**, *50*, 5070.
(38) Singh, V.; Azarkh, M.; Exner, T. E.; Hartig, J. S.; Drescher, M. *Angew. Chem., Int. Ed.* **2009**, *48*, 9728.
(39) Igarashi, R.; Sakai, T.; Hara, H.; Tenno, T.; Tanaka, T.; Tochio, H.; Shirakawa, M. *J. Am. Chem. Soc.* **2010**, *132*, 8228.
(40) Azarkh, M.; Okle, O.; Eyring, P.; Dietrich, D. R.; Drescher, M. *J. Magn. Reson.* **2011**, *212*, 450.
(41) Xue, Y.; Liu, J.-q.; Zheng, K.-w.; Kan, Z.-y.; Hao, Y.-h.; Tan, Z. *Angew. Chem., Int. Ed.* **2011**, *50*, 8046.
(42) Xu, L.; Feng, S.; Zhou, X. *Chem. Commun.* **2011**, *47*, 3517.
(43) Carr, D. H.; Brown, J.; Bydder, G. M.; Steiner, R. E.; Weinmann, H. J.; Speck, U.; Hall, A. S.; Young, I. R. *Am. J. Roentgenol.* **1984**, *143*, 215.
(44) Bottrill, M.; Kwok, L.; Long, N. J. *Chem. Soc. Rev.* **2006**, *35*, 557.
(45) Lee, J.; Zylka, M. J.; Anderson, D. J.; Burdette, J. E.; Woodruff, T. K.; Meade, T. J. *J. Am. Chem. Soc.* **2005**, *127*, 13164.
(46) Jacques, V.; Desreux, J. In *Contrast Agents I*; Krause, W., Ed.; Springer: Berlin Heidelberg, 2002; Vol. *221*, p 123.
(47) Lueders, P.; Jeschke, G.; Yulikov, M. *J. Phys. Chem. Lett.* **2011**, *2*, 604.
(48) Goldfarb, D. *Phys. Chem. Chem. Phys.* **2014**, *16*, 9685.
(49) Song, Y.; Meade, T. J.; Astashkin, A. V.; Klein, E. L.; Enemark, J. H.; Raitsimring, A. *J. Magn. Reson.* **2011**, *210*, 59.
(50) Raitsimring, A. M.; Gunanathan, C.; Potapov, A.; Efremenko, I.; Martin, J. M. L.; Milstein, D.; Goldfarb, D. *J. Am. Chem. Soc.* **2007**, *129*, 14138.
(51) Potapov, A.; Song, Y.; Meade, T. J.; Goldfarb, D.; Astashkin, A. V.; Raitsimring, A. *J. Magn. Reson.* **2010**, *205*, 38.
(52) Gordon-Grossman, M.; Kaminker, I.; Gofman, Y.; Shai, Y.; Goldfarb, D. *Phys. Chem. Chem. Phys.* **2011**, *13*, 10771.
(53) Potapov, A.; Yagi, H.; Huber, T.; Jergic, S.; Dixon, N. E.; Otting, G.; Goldfarb, D. *J. Am. Chem. Soc.* **2010**, *132*, 9040.
(54) Martorana, A.; Bellapadrona, G.; Feintuch, A.; Di Gregorio, E.; Aime, S.; Goldfarb, D. *J. Am. Chem. Soc.* **2014**, *136*, 13458.
(55) Weinmann, H. J.; Brasch, R. C.; Press, W. R.; Wesbey, G. E. *Am. J. Roentgenol.* **1984**, *142*, 619.
(56) Bousquet, J. C.; Saini, S.; Stark, D. D.; Hahn, P. F.; Nigam, M.; Wittenberg, J.; Ferrucci, J. T. *Radiology* **1988**, *166*, 693.
(57) Cacheris, W. P.; Quay, S. C.; Rocklage, S. M. *M. R. I.* **1990**, *8*, 467.
(58) Chellquist, E. M.; Searle, R. *J. Pharm. Biomed. Anal.* **1993**, *11*, 985.
(59) Schuler, B.; Lipman, E. A.; Steinbach, P. J.; Kumke, M.; Eaton, W. A. *Proc. Natl. Acad. Sci. U. S. A.* **2005**, *102*, 2754.
(60) Ungar-Waron, H.; Gurari, D.; Hurwitz, E.; Sela, M. *Eur. J. Immunol.* **1973**, *3*, 201.
(61) Polyhach, Y.; Bordignon, E.; Jeschke, G. *Phys. Chem. Chem. Phys.* **2011**, *13*, 2356.
(62) Kosen, P. A. *Methods Enzymol.* **1989**, *177*, 86.
(63) Griffith, O. H.; McConnell, H. M. *Proc. Natl. Acad. Sci. U. S. A.* **1966**, *55*, 8.
(64) Yang, Y.; Li, Q.-F.; Cao, C.; Huang, F.; Su, X.-C. *Chem.—Eur. J.* **2013**, *19*, 1097.
(65) Pellegatti, L.; Zhang, J.; Drahos, B.; Villette, S.; Suzenet, F.; Guillaumet, G.; Petoud, S.; Toth, E. *Chem. Commun.* **2008**, 6591.
(66) Molander, G. A.; Brown, A. R. *J. Org. Chem.* **2006**, *71*, 9681.
(67) Braun, S.; Kalinowski, H.-O.; Berger, S. *150 and more basic NMR experiments: A practical course*; VCH: Weinheim: New York, NY, 1998.
(68) Burns, J. A.; Butler, J. C.; Moran, J.; Whitesides, G. M. *J. Org. Chem.* **1991**, *56*, 2648.
(69) Getz, E. B.; Xiao, M.; Chakrabarty, T.; Cooke, R.; Selvin, P. R. *Anal. Biochem.* **1999**, *273*, 73.
(70) Igarashi, R.; Sakai, T.; Hara, H.; Tenno, T.; Tanaka, T.; Tochio, H.; Shirakawa, M. *J. Am. Chem. Soc.* **2010**, *132*, 8228.
(71) Lopiano, L.; Chiesa, M.; Digilio, G.; Giraudo, S.; Bergamasco, B.; Torre, E.; Fasano, M. *Biochim. Biophys. Acta* **2000**, *1500*, 306.

(72) Jeschke, G.; Chechik, V.; Ionita, P.; Godt, A.; Zimmermann, H.; Banham, J.; Timmel, C. R.; Hilger, D.; Jung, H. *Appl. Magn. Reson.* **2006**, *30*, 473.
(73) Rappe, A. K.; Casewit, C. J.; Colwell, K. S.; Goddard, W. A.; Skiff, W. M. *J. Am. Chem. Soc.* **1992**, *114*, 10024.
(74) Rucker, A. L.; Pager, C. T.; Campbell, M. N.; Qualls, J. E.; Creamer, T. P. *Proteins: Struct., Funct., Bioinf.* **2003**, *53*, 68.
(75) Knof, S.; Engel, J. *Isr. J. Chem.* **1974**, *12*, 165.
(76) Krimm, S.; Tiffany, M. L. *Isr. J. Chem.* **1974**, *12*, 189.
(77) Kuemin, M.; Engel, J.; Wennemers, H. *J. Pept. Sci.* **2010**, *16*, 596.
(78) Geisler, I.; Chmielewski, J. *Bioorg. Med. Chem. Lett.* **2007**, *17*, 2765.
(79) Fillon, Y. A.; Anderson, J. P.; Chmielewski, J. *J. Am. Chem. Soc.* **2005**, *127*, 11798.
(80) Gillespie, P. J.; Gambus, A.; Blow, J. J. *Methods* **2012**, *57*, 203.
(81) Kuemin, M.; Schweizer, S.; Ochsenfeld, C.; Wennemers, H. *J. Am. Chem. Soc.* **2009**, *131*, 15474.
(82) Horng, J.-C.; Raines, R. T. *Protein Sci.* **2006**, *15*, 74.
(83) Kakinoki, S.; Hirano, Y.; Oka, M. *Polym. Bull.* **2005**, *53*, 109.
(84) Fischer, G.; Schmid, F. X. *Biochemistry* **1990**, *29*, 2205.
(85) Lu, K. P.; Finn, G.; Lee, T. H.; Nicholson, L. K. *Nat. Chem. Biol.* **2007**, *3*, 619.
(86) Kramer, M. L.; Fischer, G. *Biopolymers* **1997**, *42*, 49.
(87) Lu, K. P.; Zhou, X. Z. *Nat. Rev. Mol. Cell Biol.* **2007**, *8*, 904.
(88) Fanghänel, J. *Front. Biosci.* **2004**, *9*, 3453.
(89) Dastvan, R.; Bode, B. E.; Karuppiah, M. P. R.; Marko, A.; Lyubenova, S.; Schwalbe, H.; Prisner, T. F. *J. Phys. Chem. B* **2010**, *114*, 13507.
(90) Kukula, H.; Veit, S.; Godt, A. *Eur. J. Org. Chem.* **1999**, *1999*, 277.
(91) Speight, J. G.; Lange, N. A. *Lange's handbook of chemistry (70th anniversary ed.)*; McGraw-Hill: New York, Toronto, 2005; Vol. 16.
(92) Murray, A. W. In *Methods in Cell Biology*; Peng, B. K. K. a. H. B., Ed.; Academic Press: San Diego, CA, 1991; Vol. *36*, p 581.
(93) Desai, A.; Murray, A.; Mitchison, T. J.; Walczak, C. E. In *Methods in Cell Biology*; Rieder, C. L., Ed.; Academic Press: Albany, NY, 1998; Vol. *61*, p 385.
(94) Neese, F. *Wiley Interdiscip. Rev.: Comput. Mol. Sci.* **2012**, *2*, 73.
(95) Martin, M. G.; Thompson, A. P.; Nenoff, T. M. *J. Chem. Phys.* **2001**, *114*, 7174.
(96) Pettersen, E. F.; Goddard, T. D.; Huang, C. C.; Couch, G. S.; Greenblatt, D. M.; Meng, E. C.; Ferrin, T. E. *J. Comput. Chem.* **2004**, *25*, 1605.